H1prelim-09-044 Submitted to

XVII International Workshop on Deep Inelastic Scattering, DIS2009, April 26-30, 2009, Madrid
Parallel Session **Structure functions**

Electronic Access: www-h1.desy.de/publications/H1preliminary.short_list.html

Measurement of the Longitudinal Structure Function F_L of the Proton at Low x in an extended Q2 range (version of April 17, 2009)

H1 Collaboration

Abstract

A measurement is presented of the longitudinal proton structure function $F_L(x, Q^2)$ derived from inclusive deep inelastic ep scattering cross section measurements with the H1 detector at HERA. The data were taken in the year 2007 at a positron beam energy of $E_e = 27.5$ GeV and proton beam energies E_p of 920 GeV, 575 GeV and 460 GeV. The measurements of F_L use different parts of the H1 detector covering when combined a range of four-momentum transfers squared $2.5 \leq Q^2 \leq 800$ GeV^2 and Bjorken x between 0.00005 and 0.035. The data are compared with higher order QCD predictions.

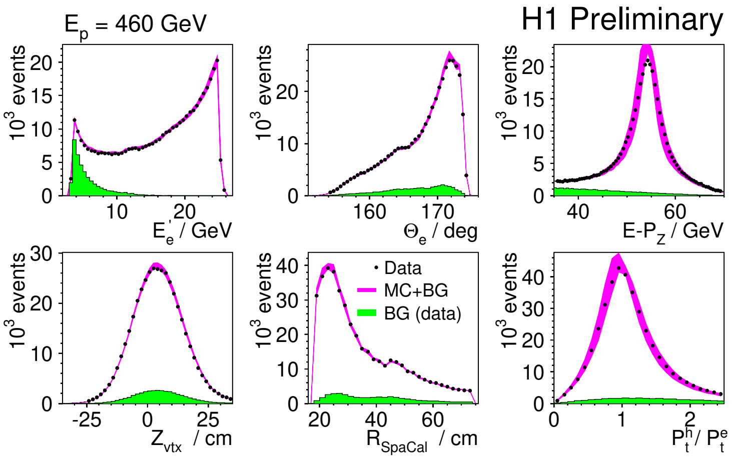

Figure 1: The comparison of the positive charge data (points) with the sum of background determined from the negative charge data (green histogram) and the DIS MC (magenta band) for the low proton beam energy (460 GeV) in the full electron energy range from 3.4 GeV to 32 GeV. The band includes statistical error on MC and background as well as correlated systematic uncertainty. The distributions from left to right and from up to down are the scattered electron energy $\mathrm{E}_\mathrm{e}^{'}$, the scattered electron polar angle Θ_e, the sum $\mathrm{E}-\mathrm{P}_\mathrm{z}$ of all final state particles, the z-position of the event vertex Z_vtx, the radial coordinate of the cluster position in SpaCal R_{SpaCal} and the P_t balance P_t^h/P_t^e.

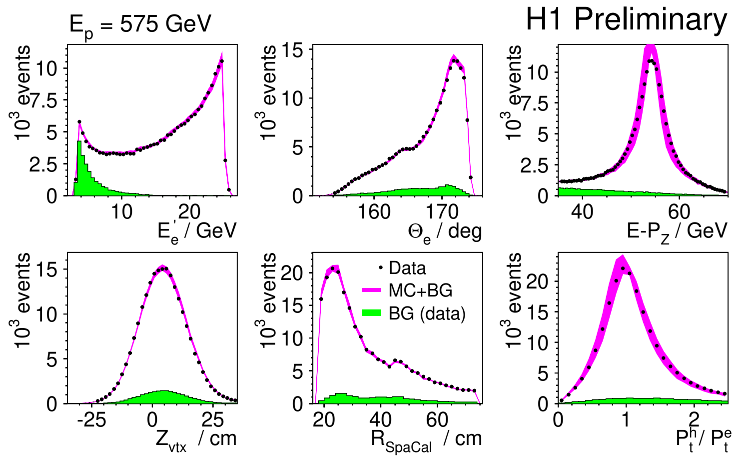

Figure 2: The comparison of the positive charge data (points) with the sum of background determined from the negative charge data (green histogram) and the DIS MC (magenta band) for the medium proton beam energy (575 GeV) in the full electron energy range from 3.4 GeV to 32 GeV. The band includes statistical error on MC and background as well as correlated systematic uncertainty. The distributions from left to right and from up to down are the scattered electron energy $\mathrm{E}_\mathrm{e}^{'}$, the scattered electron polar angle Θ_e, the sum $\mathrm{E}-\mathrm{P_z}$ of all final state particles, the z-position of the event vertex $\mathrm{Z_{vtx}}$, the radial coordinate of the cluster position in SpaCal R_{SpaCal} and the $\mathrm{P_t}$ balance P_t^h/P_t^e.

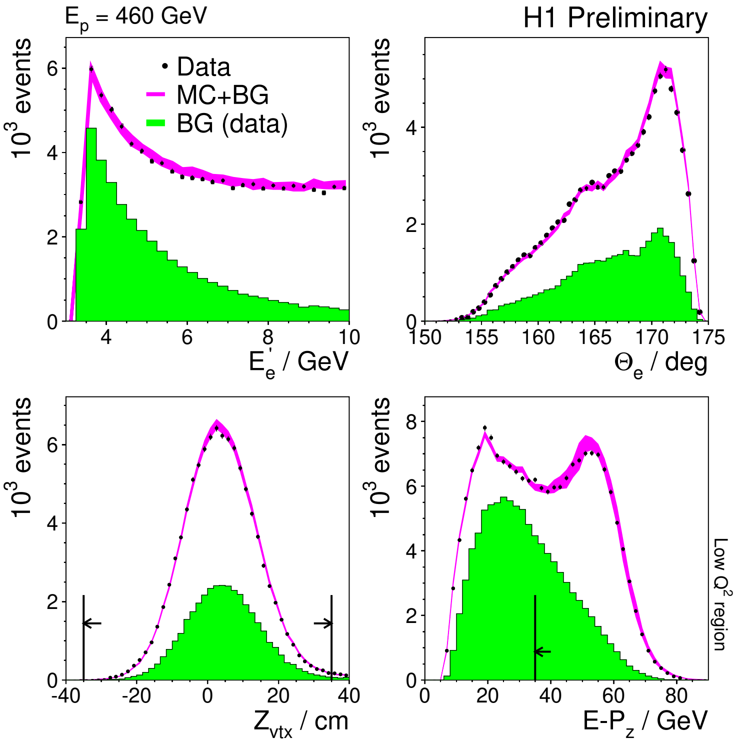

Figure 3: The comparison of the positive charge data (points) with the sum of background determined from the negative charge data (green histogram) and the DIS MC (magenta band) for the low proton beam energy (460 GeV) with the scattered electron energy less than 10 GeV. The band includes statistical error on MC and background as well as correlated systematic uncertainty. The distributions from left to right and from up to down are the scattered electron energy $\mathrm{E_e'}$, the scattered electron polar angle Θ_e, the z-position of the event vertex $\mathrm{Z_{vtx}}$ and the sum $\mathrm{E-P_z}$ of all final state particles. The cut values on the last two variables, which are applied in the analysis, are indicated by vertical lines. For $\mathrm{Z_{vtx}}$ that is range of 35 cm and for $\mathrm{E-P_z}$ cut is on 35 GeV.

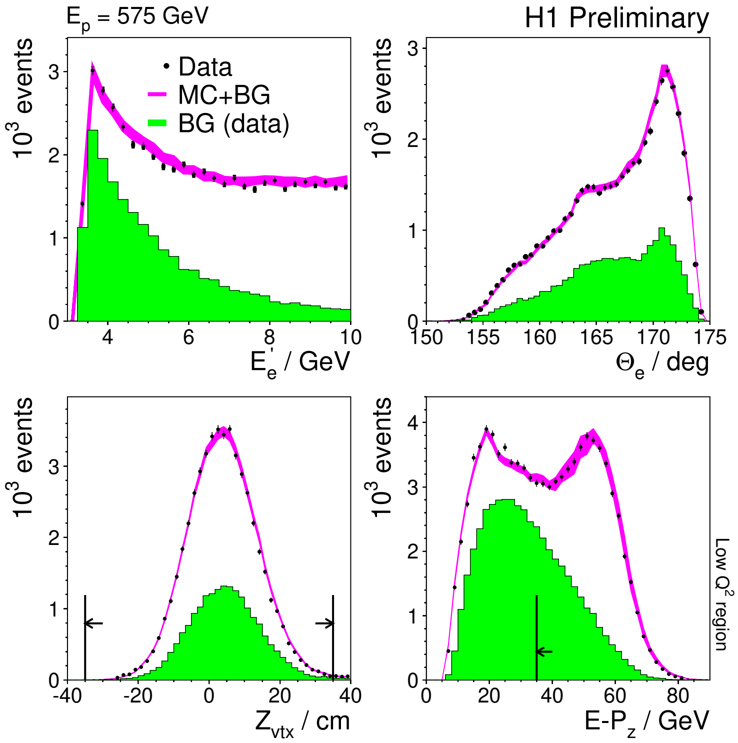

Figure 4: The comparison of the positive charge data (points) with the sum of background determined from the negative charge data (green histogram) and the DIS MC (magenta band) for the medium proton beam energy (575 GeV) with the scattered electron energy less than 10 GeV. The band includes statistical error on MC and background as well as correlated systematic uncertainty. The distributions from left to right and from up to down are the scattered electron energy $\mathrm{E}_{\mathrm{e}}^{\prime}$, the scattered electron polar angle Θ_e, the z-position of the event vertex $\mathrm{Z}_{\mathrm{vtx}}$ and the sum $\mathrm{E}-\mathrm{P}_{\mathrm{z}}$ of all final state particles. The cut values on the last two variables, which are applied in the analysis, are indicated by vertical lines. For $\mathrm{Z}_{\mathrm{vtx}}$ that is range of 35 cm and for $\mathrm{E}-\mathrm{P}_{\mathrm{z}}$ cut is on 35 GeV.

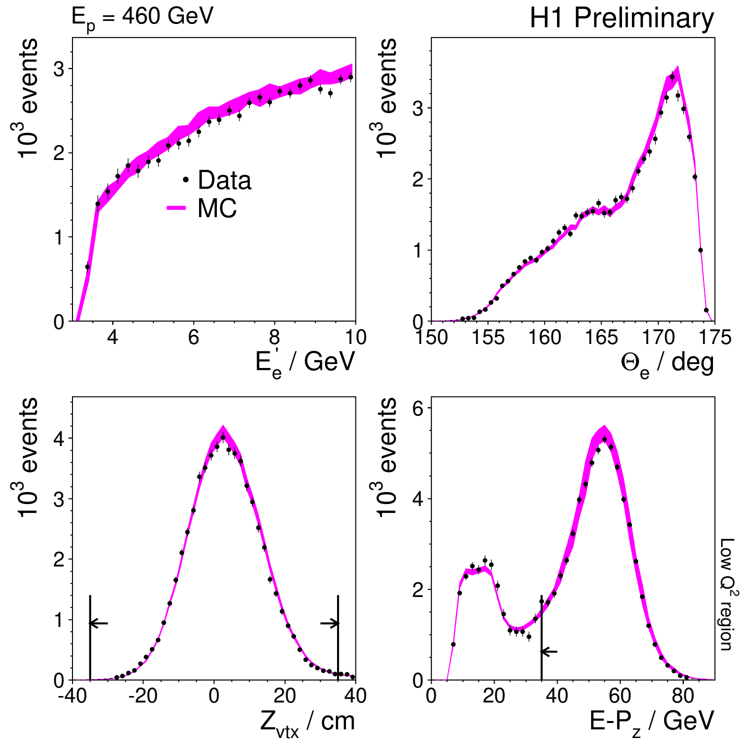

Figure 5: The comparison of the signal distributions (background subtracted with corresponding asymmetry factor) for the low proton beam energy (460 GeV) with the scattered electron energy less than 10 GeV. The distributions from left to right and from up to down are the scattered electron energy $\mathrm{E}_{\mathrm{e}}^{\prime}$, the scattered electron polar angle Θ_e, the z-position of the event vertex $\mathrm{Z}_{\mathrm{vtx}}$ and the sum $\mathrm{E}-\mathrm{P}_{\mathrm{z}}$ of all final state particles. The cut values on the last two variables, which are applied in the analysis, are indicated by vertical lines. For $\mathrm{Z}_{\mathrm{vtx}}$ that is range of 35 cm and for $\mathrm{E}-\mathrm{P}_{\mathrm{z}}$ cut is on 35 GeV.

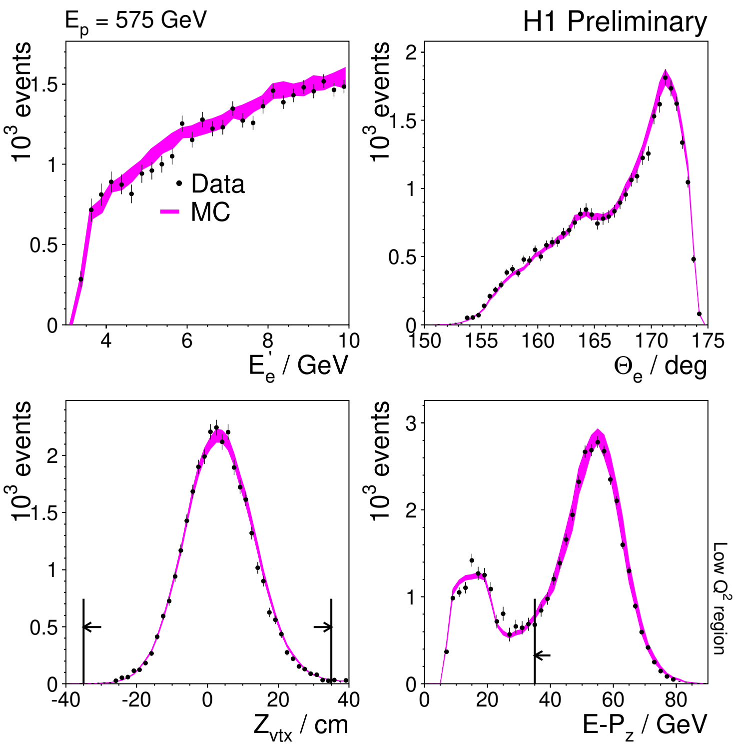

Figure 6: The comparison of the signal distributions (background subtracted with corresponding asymmetry factor) for the medium proton beam energy (575 GeV) with the scattered electron energy less than 10 GeV. The distributions from left to right and from up to down are the scattered electron energy $\mathrm{E}_{\mathrm{e}}^{'}$, the scattered electron polar angle Θ_e, the z-position of the event vertex $\mathrm{Z}_{\mathrm{vtx}}$ and the sum $\mathrm{E}-\mathrm{P}_{\mathrm{z}}$ of all final state particles. The cut values on the last two variables, which are applied in the analysis, are indicated by vertical lines. For $\mathrm{Z}_{\mathrm{vtx}}$ that is range of 35 cm and for $\mathrm{E}-\mathrm{P}_{\mathrm{z}}$ cut is on 35 GeV.

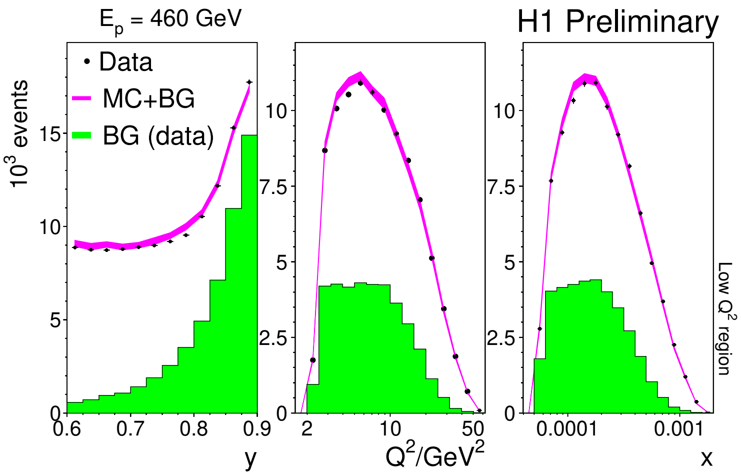

Figure 7: The comparison of the positive charge data (points) with the sum of background determined from the negative charge data (green histogram) and the DIS MC (magenta band) for the low proton beam energy (460 GeV) with the scattered electron energy less than 10 GeV. The distributions from left to right are the inelasticity y, the four-momentum transfer squared Q^2 and Bjorken x.

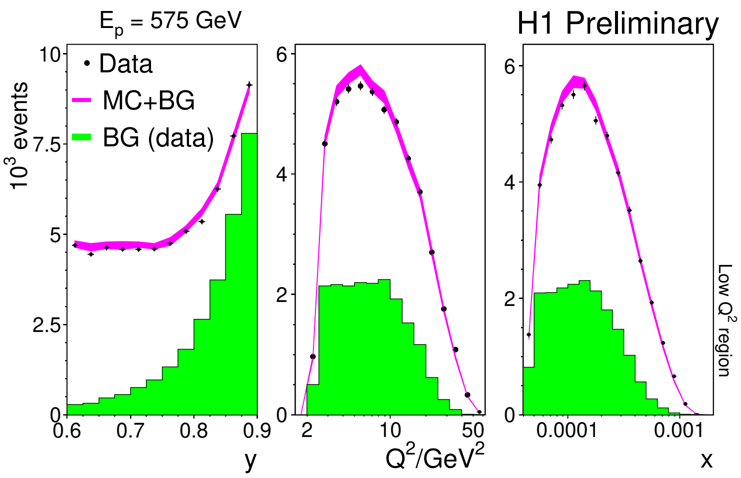

Figure 8: The comparison of the positive charge data (points) with the sum of background determined from the negative charge data (green histogram) and the DIS MC (magenta band) for the medium proton beam energy (575 GeV) with the scattered electron energy less than 10 GeV. The distributions from left to right are the inelasticity y, the four-momentum transfer squared Q^2 and Bjorken x.

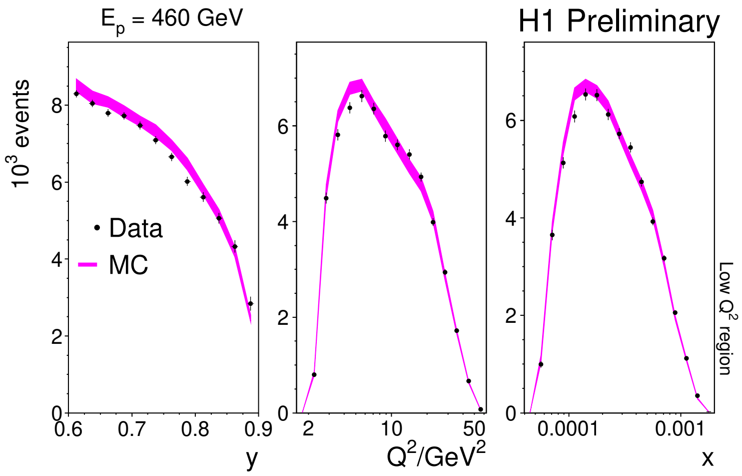

Figure 9: The comparison of the signal distributions (background subtracted with corresponding asymmetry factor) for the low proton beam energy (460 GeV) with the scattered electron energy less than 10 GeV. The distributions from left to right are the inelasticity y, the four-momentum transfer squared Q^2 and Bjorken x.

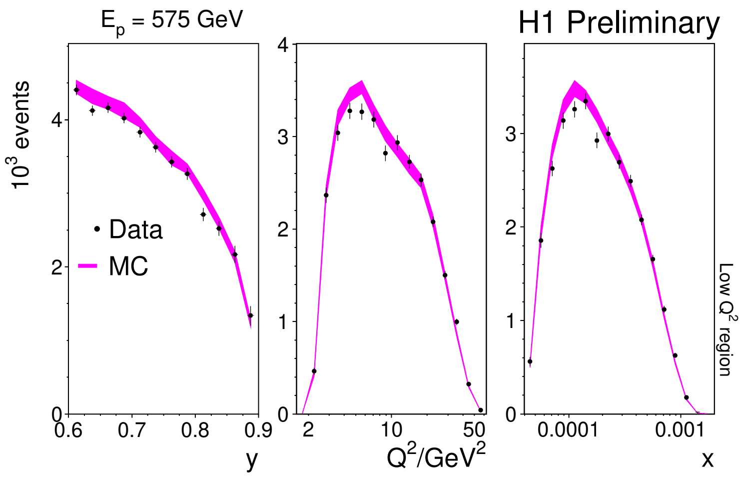

Figure 10: The comparison of the signal distributions (background subtracted with corresponding asymmetry factor) for the medium proton beam energy (575 GeV) with the scattered electron energy less than 10 GeV. The distributions from left to right are the inelasticity y, the four-momentum transfer squared Q^2 and Bjorken x.

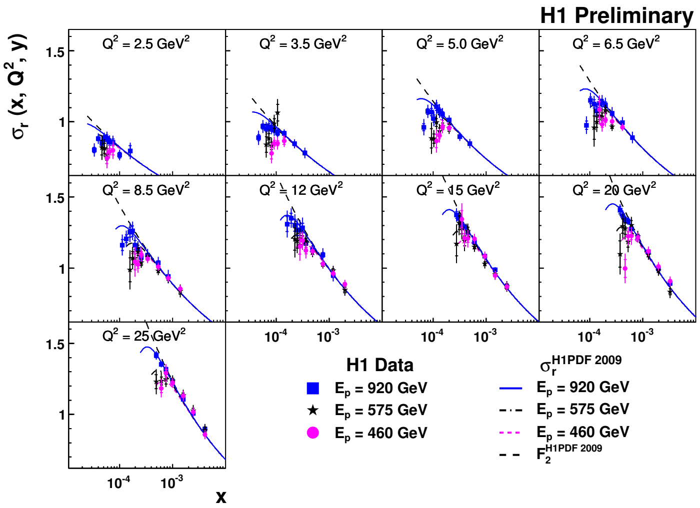

Figure 11: The reduced cross section $\sigma_r(x, Q^2, y)$ measured at different Q^2 values as a function of x using data taken at the proton beam energies of 920 GeV (boxes), 575 GeV (stars) and 460 GeV (points). The inner error bars are the statistical errors and the full error bars represent the statistical and the systematic errors added in quadrature. Theoretical predictions of σ_r are shown as the solid blue line for 920 GeV, the dashed-dotted black line for 575 GeV and the dashed magenta line for 460 GeV. The dashed black line represents the QCD expectation of F_2 derived from the H1PDF 2009 fit.

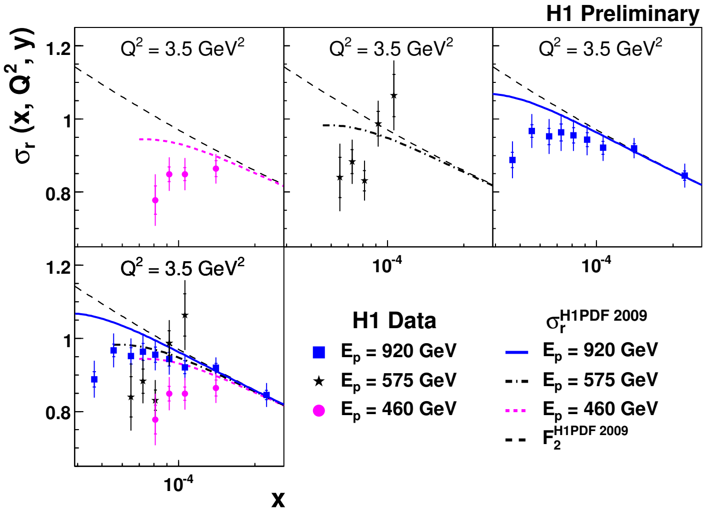

Figure 12: The reduced cross section $\sigma_r(x, Q^2, y)$ measured at $\mathrm{Q}^2 = 3.5\ \mathrm{GeV}^2$ as a function of x using data taken at the proton beam energies of 920 GeV (boxes), 575 GeV (stars) and 460 GeV (points). The inner error bars are the statistical errors and the full error bars represent the statistical and the systematic errors added in quadrature. Theoretical predictions of σ_r are shown as the solid blue line for 920 GeV, the dashed-dotted black line for 575 GeV and the dashed magenta line for 460 GeV. The dashed black line represents the QCD expectation of F_2 derived from the H1PDF 2009 fit.

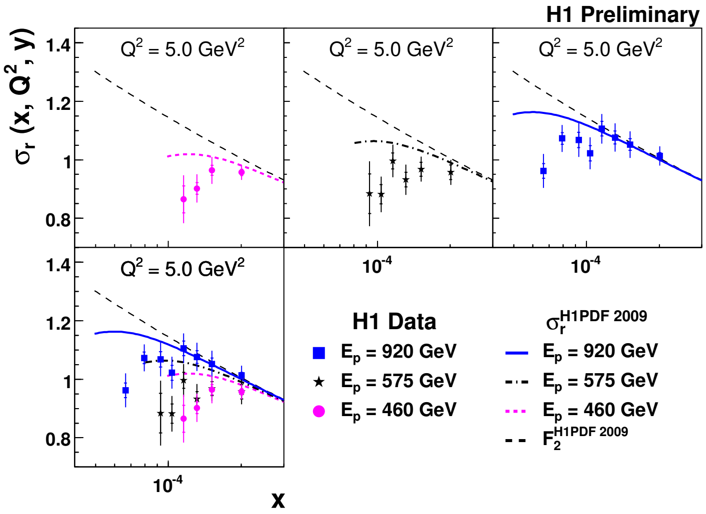

Figure 13: The reduced cross section $\sigma_r(x, Q^2, y)$ measured at $\mathrm{Q}^2 = 5\ \mathrm{GeV}^2$ as a function of x using data taken at the proton beam energies of 920 GeV (boxes), 575 GeV (stars) and 460 GeV (points). The inner error bars are the statistical errors and the full error bars represent the statistical and the systematic errors added in quadrature. Theoretical predictions of σ_r are shown as the solid blue line for 920 GeV, the dashed-dotted black line for 575 GeV and the dashed magenta line for 460 GeV. The dashed black line represents the QCD expectation of F_2 derived from the H1PDF 2009 fit.

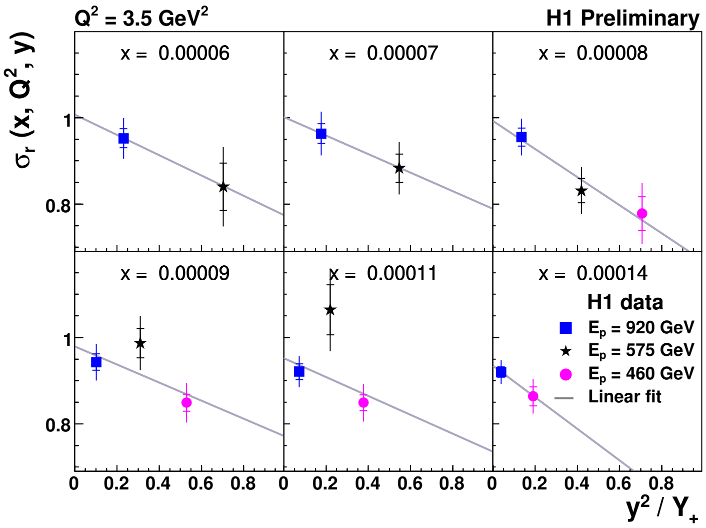

Figure 14: The reduced cross section $\sigma_r(x, Q^2, y)$ measured at $\mathrm{Q}^2 = 3.5\ \mathrm{GeV}^2$ and different values of x as a function of $y^2/[1 + (1 - y)^2]$ at the proton beam energies of 920 GeV (full boxes), 575 GeV (stars) and 460 GeV (full circles). The inner error bars are the statistical errors and the full error bars represent the statistical and the systematic errors added in quadrature. The lines are the linear fits used to determine F_L.

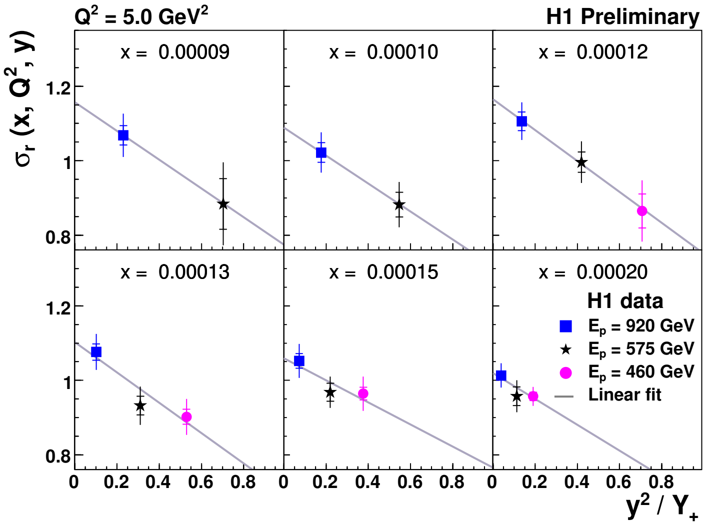

Figure 15: The reduced cross section $\sigma_r(x, Q^2, y)$ measured at $\mathrm{Q}^2 = 5\ \mathrm{GeV}^2$ and different values of x as a function of $y^2/[1 + (1 - y)^2]$ at the proton beam energies of 920 GeV (full boxes), 575 GeV (stars) and 460 GeV (full circles). The inner error bars are the statistical errors and the full error bars represent the statistical and the systematic errors added in quadrature. The lines are the linear fits used to determine F_L.

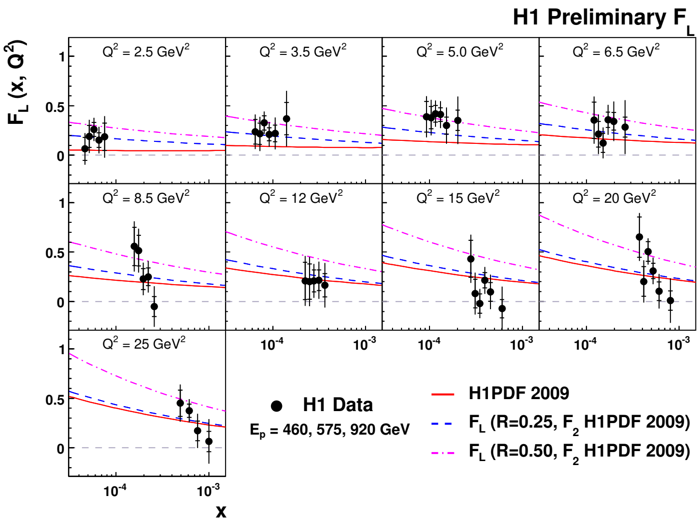

Figure 16: The longitudinal structure function F_L measured as a function of x at fixed values of Q^2. The line represents a QCD prediction of F_L from the H1PDF 2009 fit (solid red), F_L using F_2 from the H1PDF 2009 fit with $R = 0.25$ (dashed blue) and F_L using F_2 from the H1PDF 2009 fit with $R = 0.50$ (dashed dotted magenta line).

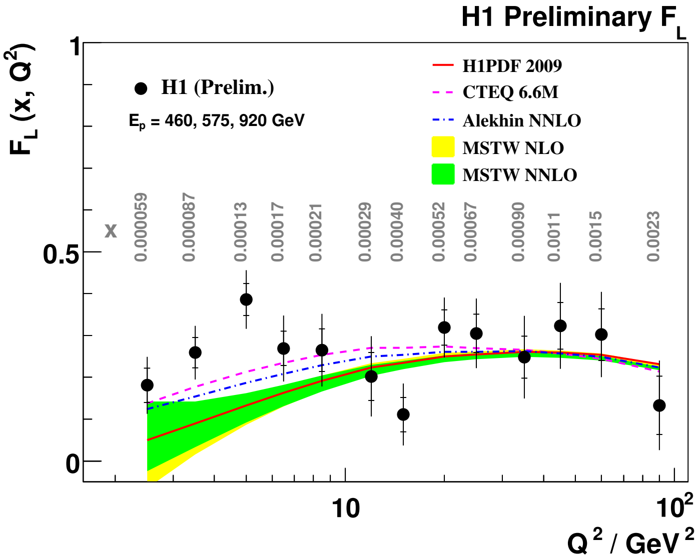

Figure 17: The longitudinal structure function F_L averaged in x at given value of Q^2 for $Q^2 < 100\ GeV^2$ using data taken at the proton beam energies of 460 GeV, 575 GeV and 920 GeV. The x values of the measurements correspondig to the Q^2-value are indicated in grey. The inner error bars are the statistical errors and the full error bars represent the statistical and the systematic erros added in quadrature. The solid red line represents a QCD prediction based on H1PDF 2009 fit, the dashed magenta line is based on CTEQ 6.6M prediction, the dashed-dotted blue line is based on Alekhin NNLO, the yellow area is based on MSTW NLO prediction and the green area is based on MSTW NNLO prediction.

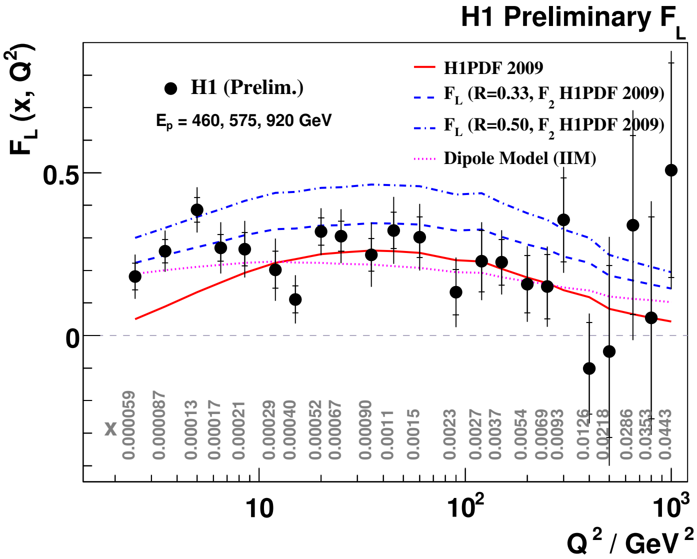

Figure 18: The longitudinal structure function F_L averaged in x at given value of Q^2 for $Q^2 < 1000\ GeV^2$ using data taken at the proton beam energies of 460 GeV, 575 GeV and 920 GeV. The x values of the measurements corresponding to the Q^2-value are indicated in grey. The inner error bars are the statistical errors and the full error bars represent the statistical and the systematic erros added in quadrature. The solid red line represents a QCD prediction based on H1PDF 2009 fit, the dashed blue line is based on H1PDF 2009 for F_2 with $R = 0.33$, the dashed-dotted blue line is based on H1PDF 2009 for F_2 with $R = 0.50$ and the dotted magenta line is based on the Dipole Model (IIM).

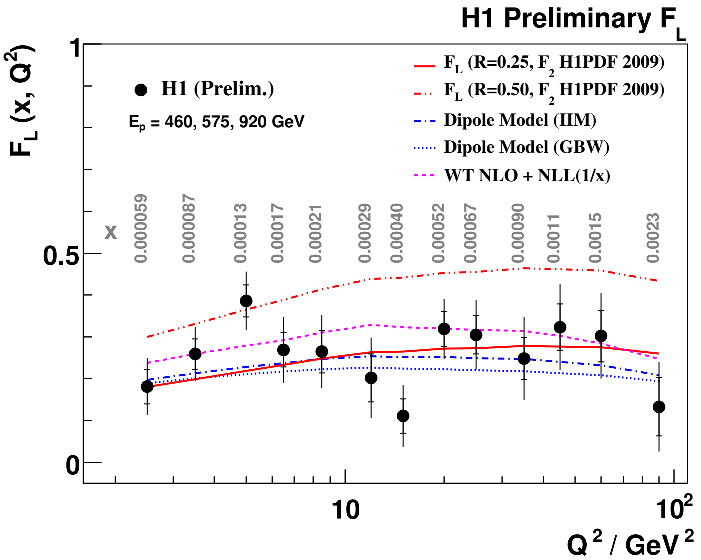

Figure 19: The longitudinal structure function F_L averaged in x at given value of Q^2 for $Q^2 < 100\ GeV^2$ using data taken at the proton beam energies of 460 GeV, 575 GeV and 920 GeV. The x values of the measurements corresponding to the Q^2-value are indicated in grey. The inner error bars are the statistical errors and the full error bars represent the statistical and the systematic erros added in quadrature. The solid red line represents a QCD prediction based on H1PDF 2009 fit for $F_2$with $R = 0.25$, the dashed-dotted red line is based on H1PDF 2009 for $F2$ with $R = 0.50$, the dashed-dotted blue is based on the Dipole Model (IIM), the dotted blue line is based on the Dipole Model (GBW) and the dashed magenta line is based on WT NLO+NLL$(1/x)$ prediction.

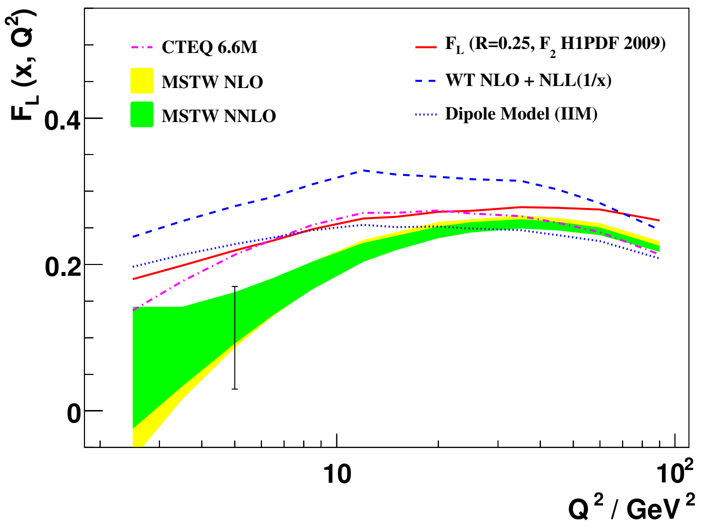

Figure 20: The longitudinal structure function F_L averaged in x at given value of Q^2 for $Q^2 < 100\ GeV^2$ using data taken at the proton beam energies of 460 GeV, 575 GeV and 920 GeV. The dashed-dotted magenta line is based on CTEQ 6.6M prediction, the yellow area is based on MSTW NLO prediction, the green area is based on MSTW NNLO prediction, the solid red line represents a QCD prediction based on H1PDF 2009 fit for F_2 with $R = 0.25$, the dashed blue is based WT NLO + NLL$(1/x)$ prediction and the dotted blue line is based on the Dipole Model (IIM).

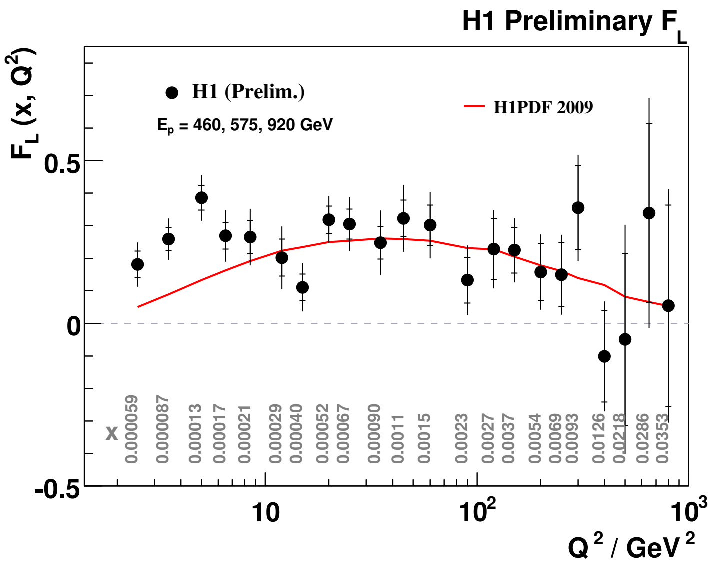

Figure 21: The longitudinal structure function F_L averaged in x at given value of Q^2 in the full range of Q^2 using data taken at the proton beam energies of 460 GeV, 575 GeV and 920 GeV. The x values of the measurements contributing to the Q^2-value are indicated in grey. The inner error bars are the statistical errors and the full error bars represent the statistical and the systematic erros added in quadrature. The solid red line represents a QCD prediction based on H1PDF 2009 fit.

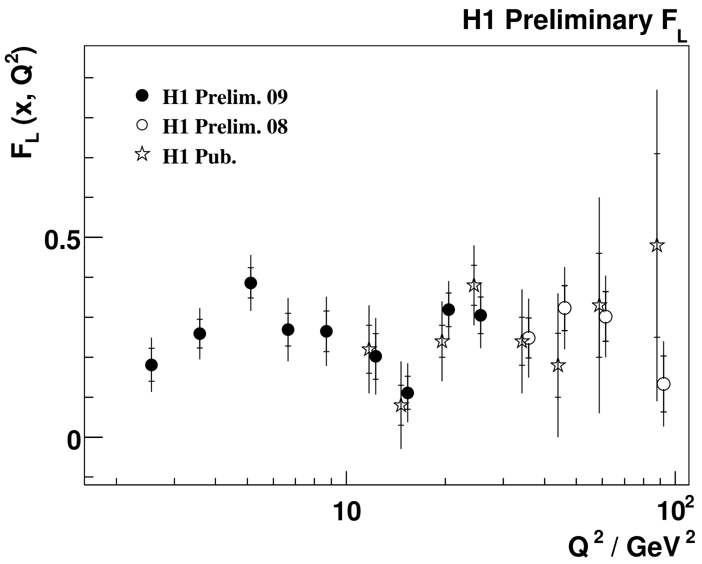

Figure 22: The comparation of the H1 Preliminary Results from the year 2009 represented with close circles (SpaCal), the H1 Preliminary Results from the year 2008 represented with open circles (combined SpaCal and LAr) and the H1 Published Results represented with open stars, in the range of $Q^2 < 100\,GeV^2$.